POLITECNICO DI TORINO
Repository ISTITUZIONALE

Dynamic analysis of a historical monumental structure due to acoustic and anthropic vibrations during large concert events

Original
Dynamic analysis of a historical monumental structure due to acoustic and anthropic vibrations during large concert events / Bali, A., Cardoni, A., Elahi, A.R., Louar, M.A., Cimellaro, G.P.. - In: JOURNAL OF CIVIL STRUCTURAL HEALTH MONITORING. - ISSN 2190-5452. - 16:6(2026). [10.1007/s13349-026-01082-5]

Availability:
This version is available at: 11583/3017750 since: 2026-11-11T12:31:22Z

Publisher:
Springer

Published
DOI:10.1007/s13349-026-01082-5

Terms of use:

This article is made available under terms and conditions as specified in the corresponding bibliographic description in the repository

Publisher copyright

(Article begins on next page)

22 November 2026

Journal of Civil Structural Health Monitoring (2026) 16:84
https://doi.org/10.1007/s13349-026-01082-5

ORIGINAL PAPER

Dynamic analysis of a historical monumental structure due to acoustic and anthropic vibrations during large concert events

Adel Bali[1,2] · Alessandro Cardoni[1] · Amir Reza Elahi[1] · Mohamed Abderaouf Louar[2] · Gian Paolo Cimellaro[1]

Received: 9 October 2025 / Revised: 11 December 2025 / Accepted: 22 June 2026
© The Author(s) 2026

Abstract

Historical monumental structures are a fundamental component of cultural identity, yet they are highly vulnerable to structural degradation driven by human activities. Among these, crowd-induced vibrations have emerged as a critical concern, particularly in historical venues that host large public events. This study investigates the structural impact of acoustic and anthropic loads on the historical Moletta Tower, located in the Circus Maximus archaeological site in Rome, Italy. A detailed three-dimensional finite element model of the tower was developed and calibrated using experimental data from a structural health monitoring campaign. The acoustic load was modeled as a periodic pressure load, while the anthropic load through a half sinusoidal model representing jumping motion of the crowd. A three-dimensional finite element model of the soil was also implemented to simulate the propagation of the crowd jumping load from the concert attendance area to the tower. A series of simulations was performed, in which the crowd size was progressively increased to assess the tower dynamic response. Structural safety was evaluated by tracking the formation of plastic hinges and comparing simulation results in terms of maximum accelerations and peak particle velocity with limits established by national regulations. Results indicate that while the effect of acoustic loads is negligible, the jumping motion of the audience can potentially pose a risk of damage for the tower. It is observed that once a certain crowd size is exceeded, localized plastic hinges begin to form, highlighting the need for proactive management strategies. By integrating analytical, experimental, and numerical methods, this research offers framework for supporting decision-makers with evidence-based policies that balance entertainment events with preservation of historical monumental structures.

Keywords Acoustic loads · Anthropic loads · Structural health monitoring · Historical structures · Cultural heritage · Three-dimensional finite element modeling

1 Introduction

Historical monumental structures are invaluable cultural assets that represent the heritage of populations across different eras, making their preservation critically important. Some of these ancient structures are still being used to this day for their intended function, although they are being subjected to increased loading levels such as pedestrian [1] and traffic loads [2]. Besides the increase of everyday loads, some monumental buildings are located nearby venues hosting large entertainment events such as concerts, which means additional exposition to intense acoustic and anthropic loads.

Several studies have aimed to develop reliable and practical models of loads generated by people jumping, typically by simulating force time-history functions in the vertical direction. Bachmann and Ammann [3] (1987) were

✉ Gian Paolo Cimellaro
gianpaolo.cimellaro@polito.it

Adel Bali
adel.bali@polito.it

Alessandro Cardoni
alessandro.cardoni@polito.it

Amir Reza Elahi
amir.elahi@polito.it

Mohamed Abderaouf Louar
r.louar@gmail.com

[1] Department of Geotechnical, Structural and Civil Engineering, Politecnico Di Torino, Turin, Italy

[2] Department of Mechanical Engineering, Ecole Militaire Polytechnique, Algiers, Algeria

Published online: 07 September 2026

among the first to investigate this phenomenon. They proposed that a series of identical half-sine wave pulses could effectively represent measured jumping-force pulses. Subsequent studies suggested that, for dynamic analysis, such periodic half-sine pulses can also be modelled using a Fourier series, where the fundamental harmonic corresponds to the jumping frequency [4, 5]. However, Racic and Pavic [6] compared the half-sine wave function with a Fourier series composed of six harmonic terms for representing the force-time history of jumping and found that, under identical conditions, such as jumping frequency and impact duration, the amplitude predicted by the Fourier-based model was lower than that of the half-sine model. Thus, the half-sine model is more conservative. The impact of this type of loading has been extensively investigated, with studies demonstrating its potentially detrimental effects on various types of structures such as stadiums [7, 8]. However, when dealing with historical towers made of masonry and heterogeneous materials, engineers and researchers face the additional challenge of properly modelling the material properties.

The rapid advancement of computational technologies has significantly enhanced the ability to simulate characteristics such as the heterogeneous composition, nonlinear material behavior, and geometric irregularities, with greater precision and efficiency [9–12]. Finite element (FE) modeling has played a crucial role in understanding the seismic behavior of historical masonry towers. Both micro-modeling and macro-modeling approaches have been employed. Micro-modeling approaches involve the detailed discretization of masonry components, allowing for a precise representation of the material behavior at a small scale [13, 14]. The use of non-smooth contact dynamics methods has also been explored for damage assessment in historical masonry structures [15]. Instead, macro-modeling approaches treat masonry as a continuum material, simplifying the analysis while still capturing overall structural behavior. This approach has been widely used for dynamic and seismic analyses of historical towers, particularly when dealing with complex geometries [16, 17]. Nonetheless, these simplified approaches could also lead to overlooking some critical failure mechanisms, especially in the case of masonry structures retrofitted with inadequate interventions [18]. Additionally, smeared damage is a common representative model of nonlinear behavior of masonry. This model was developed by Lubliner et al. [19] in 1989 and was later enhanced by Lee and Fenves [20] in 1998. The key points of this model could be calculated from masonry quality index method (MQI) as detailed by Borri et al. [21]. Masonry towers often experience high vertical compressive stress due to gravity loads, which, when combined with lateral loads induced by anthropic loads, could lead to flexural stress, shear, and ultimately cracking. Under repeated load cycles this could lead to a weakening of wall-to-wall and floor-to-wall connections, which could in turn result in common out-of-plane failures [22, 23]. Damage evolution during seismic events has been studied extensively, with particular attention paid to the role of crack propagation in reducing the structural integrity of the towers [24–26].

To calibrate the models, given that in most cases it is not possible to perform destructive tests on historical assets, structural health monitoring (SHM) campaigns are typically carried out by installing sensors that record accelerations. The recorded accelerograms are then processed using output-only operational modal analysis (OMA) methods, such as frequency domain decomposition (FDD) [27] and stochastic subspace identification (SSI) [28], enabling the identification of key dynamic properties, including natural frequencies, damping ratios, and mode shapes. Many researchers have utilized OMA to calibrate FE models by comparing the natural frequencies and mode shapes obtained experimentally with those predicted numerically [29, 30].

Although numerous studies have investigated the dynamics of masonry towers, they have done so primarily in the context of seismic loading, while the effects of anthropic vibrations generated by large crowds and acoustic vibrations during concerts remain largely overlooked in the literature. This represents a critical gap, particularly for historic structures located near entertainment venues. Therefore, the key novelty is proposing a methodology to ensure the safety of the historical monuments by combining the analytical, numerical and experimental approaches.

In this study, the archaeological site of the Circus Maximus in Rome, Italy, is used as a case study to investigate the effects of such vibrations. The Circus Maximus serves as a multifunctional entertainment venue hosting major cultural and sporting events. In recent years, the venue has hosted large concerts in July 2023, May and September 2024, and May 2025. These high-attendance events generate local ground vibrations that propagate through the soil to nearby monumental structures, particularly the Moletta Tower, located approximately 400 m from the stage area (Fig. 1).

The present research directly focuses on how dynamic loads generated by acoustic vibrations and large crowds jumping may influence the structural integrity of the Moletta Tower. A detailed non-linear FE model was developed and calibrated to simulate scenarios where people jump during events using MIDAS FEA NX software to assess the impact of these physical human activities on the tower. This model incorporates both the tower's structural characteristics and the surrounding soil-structure interaction, allowing for a realistic simulation of crowd-induced vibrations and their potential impact on the tower's structural integrity and stability.

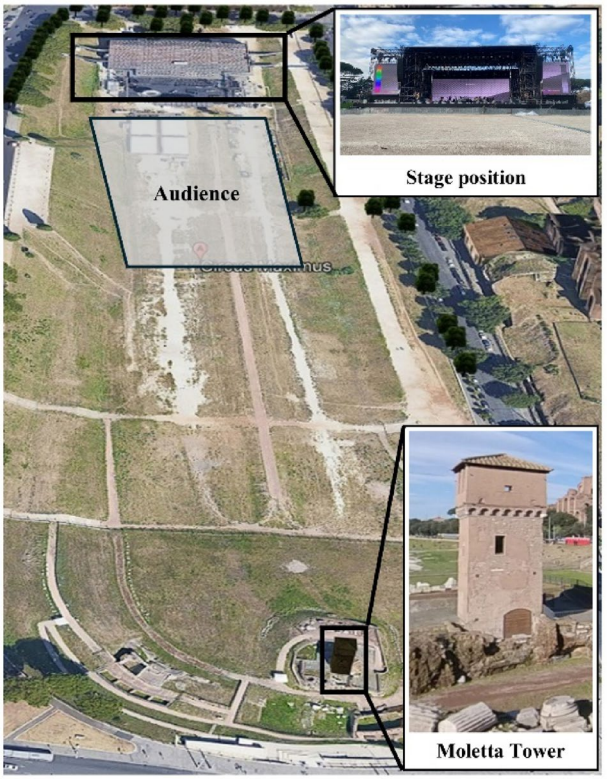


Fig. 1 Aerial view showing the location of the Moletta Tower within the Circus Maximus site

The article is articulated in two main parts. Section 2 describes the implementation of the 3D FE model of the tower that was developed to assess its structural behavior, considering the mechanical properties of masonry and soil. SHM and visual investigations were conducted to calibrate and validate the model, ensuring accurate simulation of the tower's dynamic behavior. In Sect. 3, the implementation of the Circus Maximus FE model is described, including data obtained from previous experimental works [31–34]. The dynamic loads representing acoustic and anthropic vibrations are then modelled and used as input to observe their impact on the structure. The FE model was validated by comparing the recorded accelerations during one concert event. Moreover, a sensitivity analysis was performed to measure the effect of the crowd size on the peak particle velocity (PPV), maximum accelerations at the base and the top of the tower, and formation of plastic hinges. The flowchart in Fig. 2 illustrates the methodology followed in this paper.

2 Structural characterization of the medieval Moletta Tower

This section establishes the mechanical properties and nonlinear behaviour characteristics of the masonry the tower is made of. These material properties will subsequently be applied in Sect. 3 to analyse and evaluate the structural response of the tower under human crowd loading conditions.

2.1 Geometric survey

The 14.4 m tower has a footprint of about 20 m2. The masonry walls are constructed with a non-uniform

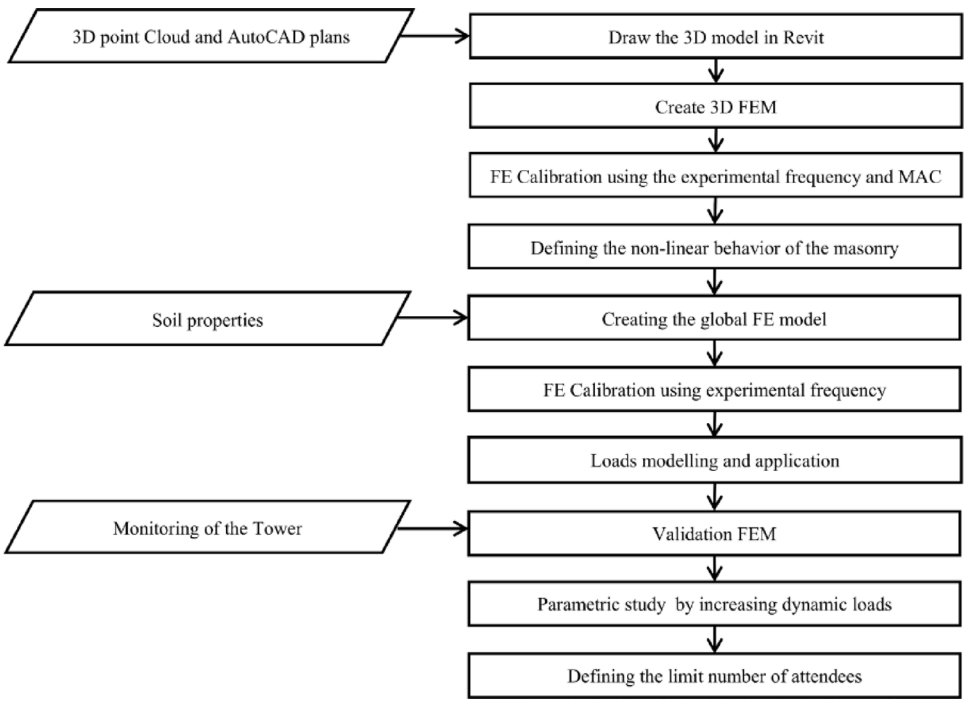


Fig. 2 Methodology followed in this work

cross-section, resulting in three distinct discontinuities. The thickness progresses from a maximum of 0.9 m at the foundation, tapering down to 0.75 m at the base and further to 0.5 m in the intermediate section. However, the upper walls thicken again to 0.7 m. Figure 3a shows the LiDAR point cloud and the numerical 3D model implemented in Revit.

The longitudinal cross-section shows the geometrical details (Fig. 3b), while the cross sections in Fig. 3c, d and e show the dimensions of the tower at the foundations, first, and second level.

2.2 Finite element model of the tower

The 3D finite element model of the tower and the surrounding soil was implemented in Midas FEA NX (Fig. 4). The mesh size is 0.25 m for the masonry walls and 0.40 m for the

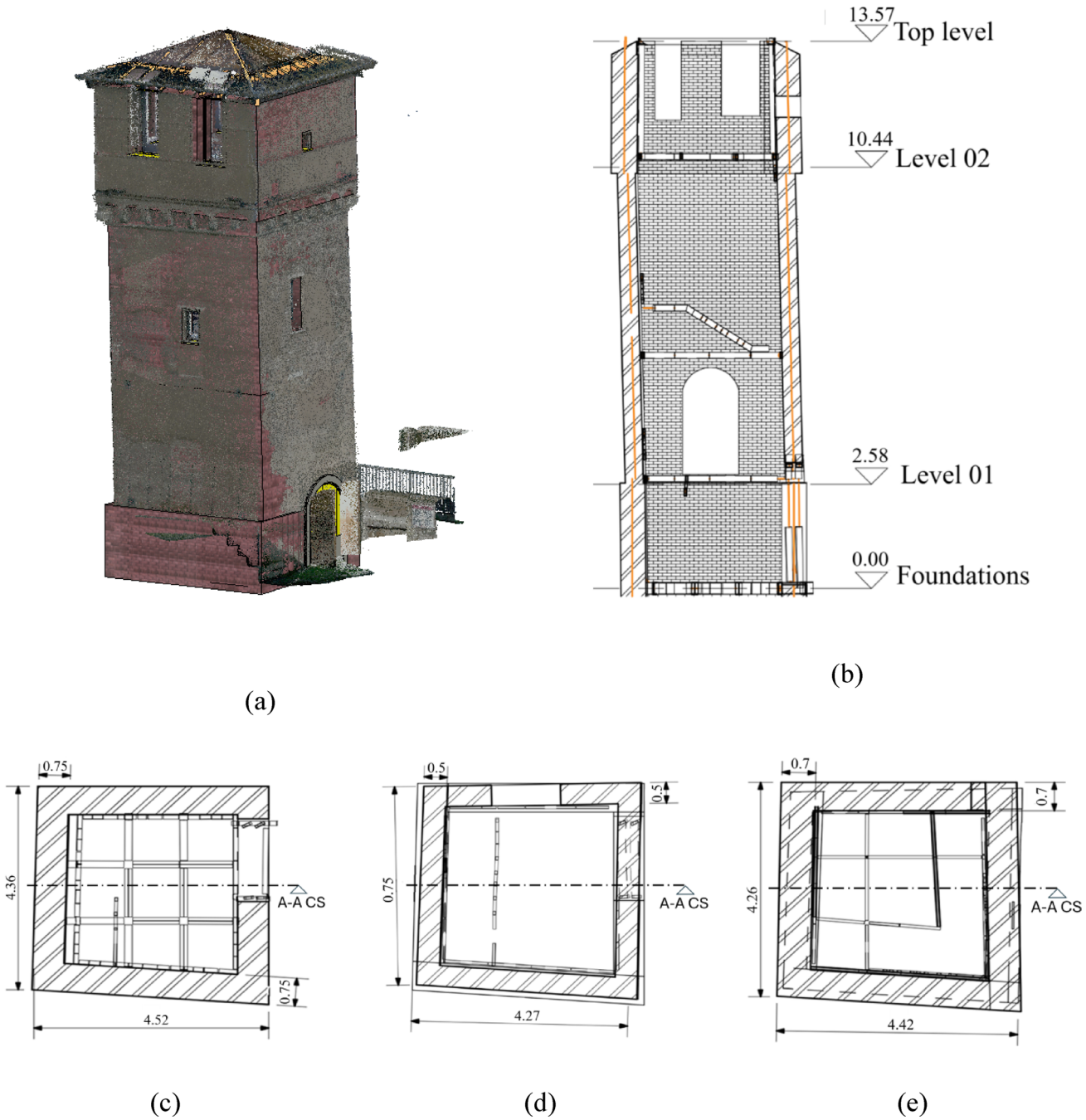


Fig. 3 Geometrical details of the model: **a** 3D LiDAR point cloud, **b** A-A elevation cross section, **c** Foundation plan view, **d** Level 01 plan view and **e** Level 02 plan view

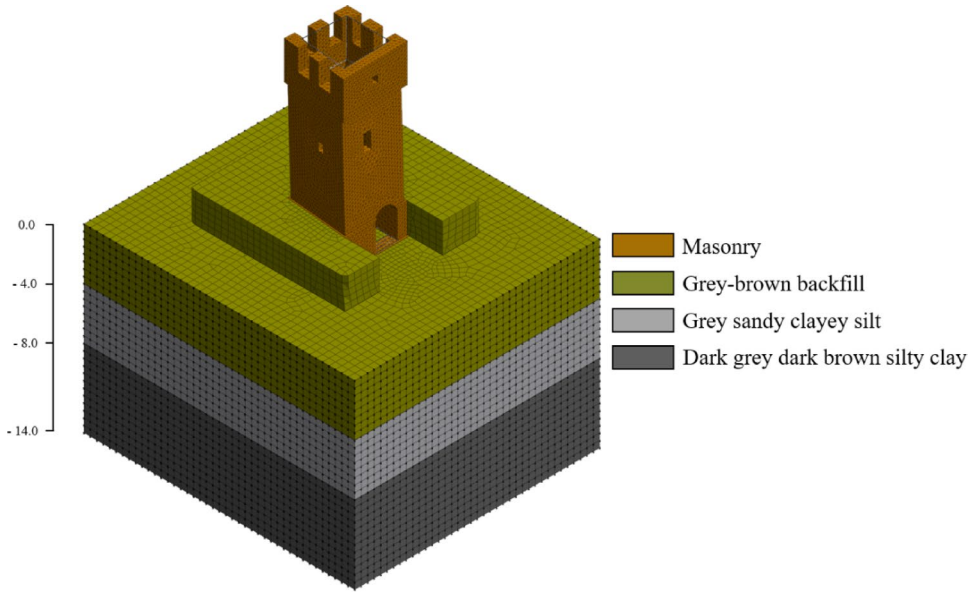


Fig. 4 3D FE model of the Moletta Tower

soil. The damping ratio for the masonry walls was set at 5% according to the literature [35].

2.3 Convergence analysis and parametric sensitivity study for finite element modeling

Convergence studies in finite element analysis serve to validate numerical solutions by demonstrating mesh independence through systematic refinement, ensuring results are not distorted by discretization errors [36]. The process evaluates key parameters such as stress, displacements and fundamental frequency, until successive refinements yield changes below an error threshold (less than 5%), balancing accuracy and computational efficiency. However, excessive refinement introduces diminishing returns, where element sizes below an optimal point yield negligible accuracy gain (e.g., 1 to 2%) while exacerbating numerical instabilities and computational burdens [37]. Adaptive meshing strategies [38] and convergence criteria are recommended to optimize this trade-off. To achieve an accurate FE representation of the tower's structural behaviour, an optimal mesh configuration is determined through systematic convergence analysis. This study evaluates mesh sensitivity by progressively refining the discretization of solid elements, i.e., masonry walls and soil, while monitoring the convergence of the fundamental natural frequency (f_1) as the primary validation parameter. The methodology involves: (1) parameterizing the mesh density through nodal count variation, (2) quantifying the relative error $\left(\varepsilon = \left|f_1^i — f_1^{i-1}\right| / f_1^{i-1}\right)$ between successive refinements, and (3) establishing convergence when ε falls below an acceptable threshold. This approach ensures mesh-independent results while maintaining computational efficiency through identification of the asymptotic region in the f_1 versus degrees-of-freedom (DOF) relationship. The main characteristics of the mesh are 7,380 nodes, 15,658 elements, 24,098 DOF, and 21,747 equations.

Table 1 Mechanical properties of the masonry walls computed by MQI method

	f_m [MPa]	f_s [kPa]	E [MPa]	G [MPa]
Mean value	3.54	73.4	1402.3	468.6

2.4 Identification of the mechanical properties

Due to the absence of data about the mechanical properties of the masonry walls and the impossibility of performing destructive testing on such historical structure, the MQI was adopted [21]. The MQI assesses the properties of historic masonry walls based on visual surveys, in accordance with construction standards. It provides valuable information about mechanical characteristics through parameters such as compression strength (f_m), shear strength (f_s), Young's modulus (E) and shear modulus (G). According to the methodology proposed in [21], it is possible to define mean values of the MQI for each parameter as shown in Table 1.

The mean value of each parameter is the tentative value used first in the FE model. These are subsequently varied during the calibration process, while verifying that they remain within the ranges of acceptable values provided by the national design codes NTC2018 [35]. NTC2018 provides values distinguishing between different types of masonry. Based on visual inspection, heterogeneity was observed in masonry wall textures, stone sizes, bonding patterns, and mortar quality (Fig. 5). The reference values for these masonry types are presented in Table 2. The average between the minima and maxima of the two masonry types



Fig. 5 Visual inspection of the masonry walls

Table 2 Mechanical properties of the masonry walls according to NTC 2018

Type of masonry	f_m [MPa]	f_t [MPa]	E [MPa]	G [MPa]	W [kN/m^3]
	Min–Max	Min–Max	Min–Max	Min–Max	
Masonry with rough-hewn ashlars, with facing of limited thickness and internal core	2.00 3.00	0.35 0.51	1020 1440	340 480	20
Solid brick and lime mortar masonry	2.40 4.00	0.60 0.92	1200 1800	400 600	18

Table 3 Mechanical properties of adjacent soil

Soil layers	γ [KN/m^3]	C' [kPa]	Cu [kPa]	Φ' [°]	E' [kPa]
Level 1: Grey-brown backfill	16–19	0–3	–	26–30	2896
Level 2: Gray sandy clayey silt	16.69–17.59	3–28	51–81	24–32	5106–5543
Level 3: Dark gray dark brown silty clay	15.1	–	64	–	2355

was calculated to define an equivalent masonry type used as reference in the model.

The steel ring beams and staircase visible in Fig. 5 were added as part of a retrofit intervention in 2013. Therefore, the properties of the steel beams used in the tower are taken from technical sheet of steel properties from EUROCODE3 [39].

Table 3 presents the geotechnical properties of three soil layers of the soil surrounding the tower, including unit weight (γ), effective cohesion (C'), undrained shear strength (Cu), internal friction angle (Φ'), and the oedometer modulus (E'), which characterizes the soil's stiffness under one-dimensional compression. The values of the considered properties were taken from [31].

2.5 Dynamic characterization

To gather the vibration data, a structural health monitoring campaign was carried out. The positions and numbers of the accelerometers are illustrated in Fig. 6. In addition, another sensor was placed close to the stage (S_53) to record the human-induced vibrations during the concert under the stage. The accelerations were recorded continuously over a seven-days period, from 29 April to 7 May , 2024, when a series of concerts took place.

To identify the dynamic characteristics of the tower, the FDD method is adopted. FDD is an output-only modal identification technique that extracts natural frequencies and mode shapes by analyzing the spectral content of ambient vibration responses. The method relies on the decomposition of the power spectral density (PSD) matrix of the system's responses using singular value decomposition (SVD). This decomposition isolates the dominant vibration energy at each frequency and effectively breaks down the system's spectral response into a set of single degree of freedom (SDOF) like components.

At each discrete frequency $\omega = \omega_i$ the estimated output PSD matrix $\hat{G}_{yy'}(j\omega_i)$ is decomposed as summerized in the Eq. 1.

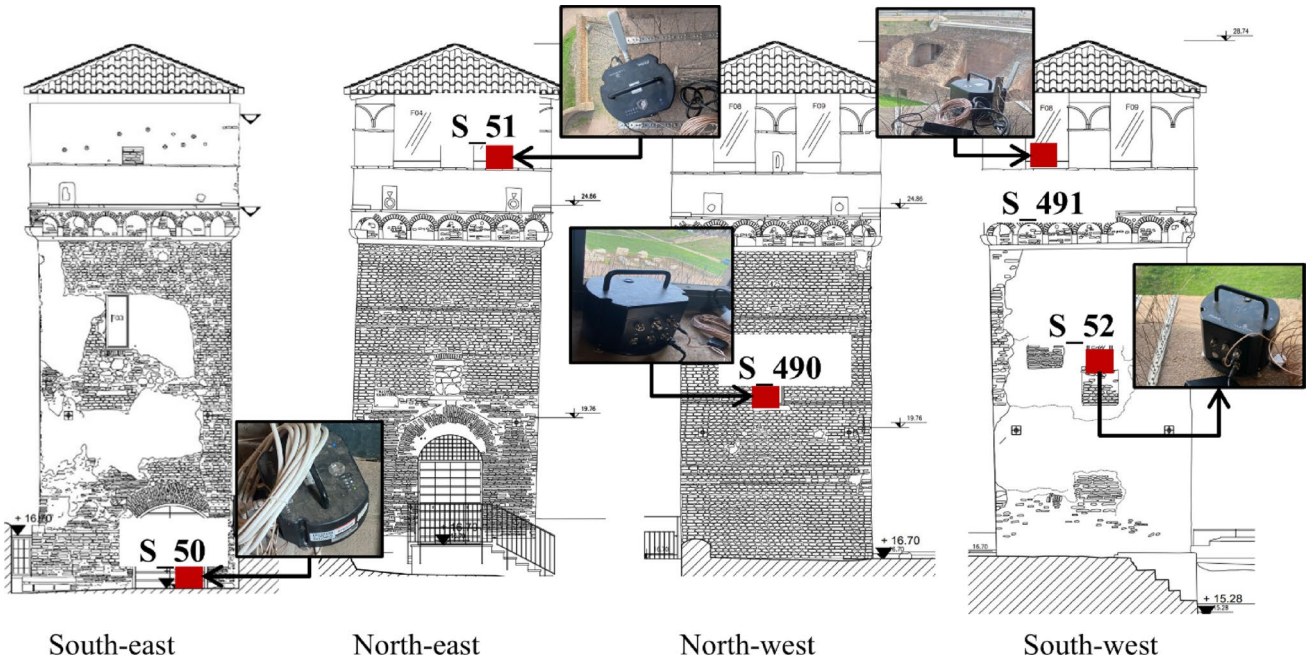


Fig. 6 Sensor layout of the SHM data acquisition campaign

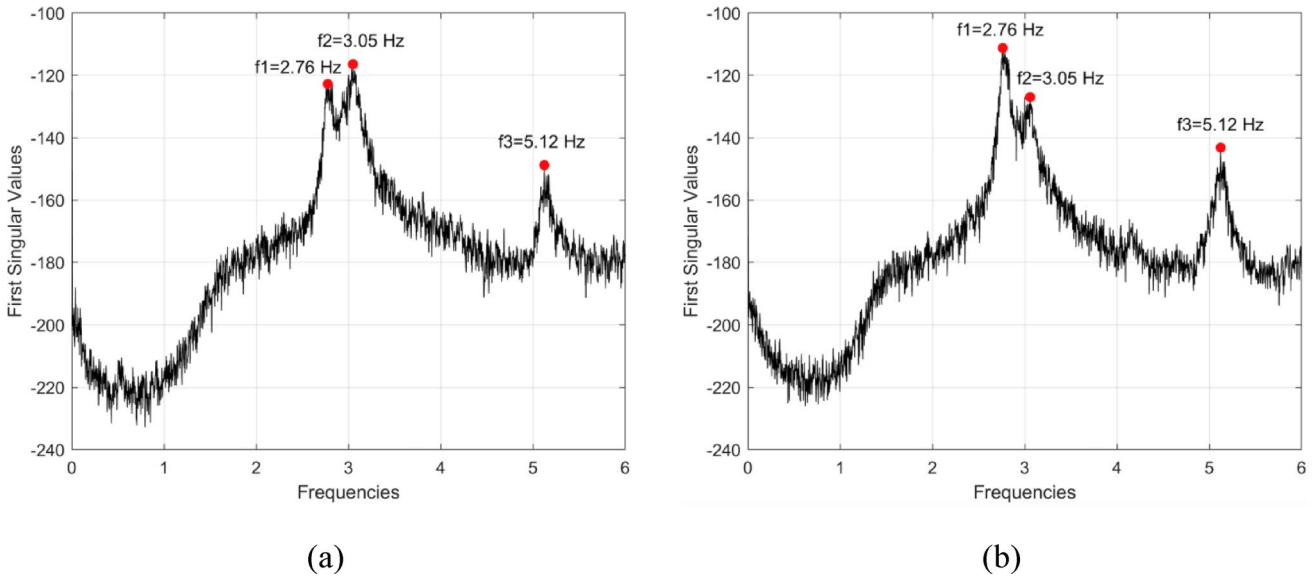


Fig. 7 Selected peaks in the SVD spectrum obtained from the ambient vibration response, (a) x-direction, (b) y-direction

$$\hat{G}_{yy}(j\omega_i) = U_i S_i U_i^T \tag{1}$$

where U_i is the unitary matrix containing the singular vectors, and S_i is the diagonal matrix containing the singular values S_{ij}.

In the singular value spectrum, resonance peaks appear at the system's natural frequencies, i.e., the characteristic frequencies at which the structure tends to vibrate when dynamically excited. Each peak corresponds to a specific vibration mode. At the frequency where a peak occurs, the dominant singular vector provides an estimate of the corresponding mode shape, which represents the deformation pattern of the structure at that natural frequency.

In the process of modal identification, the ambient vibration signals recorded between 4:00 and 4:30 UTC on May 1st, 2024 were used as input.

Figure 7 presents selected peaks in the SV spectrum and the corresponding identified modal frequencies after performing the FDD analysis. In the X direction, the SVD spectrum exhibits three distinct peaks, corresponding to the modes at 2.76 Hz, 3.05 Hz, and 5.12 Hz, respectively.

Table 4 Comparison of frequencies before and after calibration

Modes	FE model frequencies [Hz]		Experimental frequencies [Hz]	Difference between frequencies [%]	
	Before calibration	After calibration		Before calibration	After calibration
1	3.31	2.78	2.76	19.1	0.7
2	3.85	2.9	3.05	26	4.9
3	6.99	5.94	5.12	36	15

Table 5 Modal mass of the first three modes

Modes	Translation-X	Translation -Y	Rotation-Z
	Mass (%)	Mass (%)	Mass (%)
1st	6.754	48.039	3.980
2nd	49.437	6.843	3.345
3rd	3.210	2.900	59.098

These peaks appears identically present in the Fig. 7b, confirming that the identified modes participate in both X and Y directions. These values are consistent with a previous study conducted by Cardoni et al. [40]. The frequencies and mode shapes obtained from the recorded accelerograms through FDD analysis, were considered as reference for the calibration of the FE model.

The calibration was performed by varying the elasticity modules of masonry walls until a good agreement is attained. Before the calibration, i.e., Using the initial parameter value, defined as the mean Young's modulus estimated through the MQI method. differences between numerical and experimental frequencies of first, second and third modes were 19.1%, 26% and 36%, respectively. The Young's modulus of the masonry walls decreased from 1402 to 1150 MPa. After updating, differences between numerical and experimental frequencies of first, second and third modes were 0.7%, 4.9% and 15%, respectively. The first three numerical and experimental natural frequencies, for the calibrated and non-calibrated models, are presented in Table 4. The comparison between the first two numerical and experimental frequencies in the main directions shows good agreement. However, more discrepancies were found between the numerical and experimental frequencies in the torsional mode. Specifically, the model appears to be stiffer than the actual structure in the torsional mode. This difference might be related to several factors such as the heterogeneity of the materials along the height of the tower, the anisotropy of masonry, the various textures on the walls of the tower.

Table 5 shows the characteristics of the first three vibrational modes, while Fig. 8 represents the deformed shapes of the first three modes after the calibration. The 1st mode displays primary translation along the global Y-axis, the 2nd mode features dominant X-direction translation, and the 3rd mode exhibits torsional deformation around the vertical Z-axis. These modal patterns are in agreement with typical tower behavior, where lower modes show translational responses while higher modes introduce torsional effects.

The modal assurance criterion (MAC) [41] was used to compare the deformed shape vectors obtained from the experimental and numerical analyses. It is defined in Eq. 2, where φ_{FE} and φ_{exp} represent the FE model and

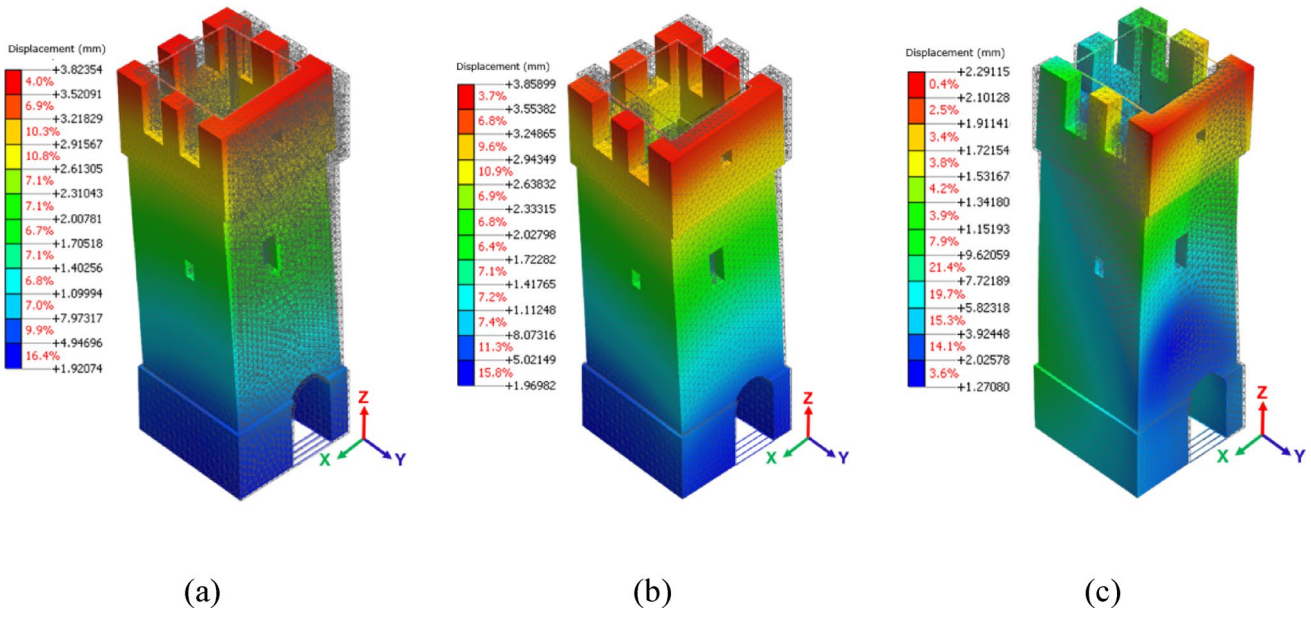


Fig. 8 Calibrated mode shapes obtained from the FE model: **a** 1st mode, **b** 2nd mode and **c** 3rd mode

experimental mode shapes respectively. The numerical model eigenvectors components are taken from the nodes corresponding to the sensor positions.

$$MAC(exp, FE) = \frac{\left|\{\varphi_{\exp}\}^T \cdot \{\varphi_{\mathrm{FE}}\}\right|^2}{\left(\{\varphi_{\exp}\}^T \cdot \{\varphi_{\exp}\}\right)\left(\{\varphi_{\mathrm{FE}}\}^T \cdot \{\varphi_{\mathrm{FE}}\}\right)} \quad (2)$$

MAC values were calculated among the modal residues extracted from the experimental analysis and the ones given by the numerical model in the same points where measurements were taken. The MAC coefficient is 0.92 for the 1st mode, 0.90 for the 2nd, and 0.89 for the 3rd, indicating a high level of matching between the experimental and numerical mode shapes.

2.6 Nonlinear properties of the material after calibration

After calibration, Young's modulus E was updated, and a new MQI was computed. The remaining material parameters were then adjusted accordingly, verifying that all values fell within the ranges specified by the NTC 2018 standard as detailed in Sect. 2.4.

The resulting maximum elastic strength values were 3.26 MPa in compression, 0.33 MPa in tension, and 0.078 MPa in shear. Figure 9 presents the stress–strain relationships characterising the mechanical behavior of the material under tension, compression, and shear, as derived from the literature [42]. These constitutive models serve as the foundation for simulating the nonlinear response of masonry in FE analyses. Figure 9a depicts the tensile stress-strain behavior of masonry. The sharp rise to a peak followed by a rapid drop illustrates the brittle failure characteristic of masonry in tension. Figure 9b shows the compressive stress-strain response. It highlights more ductile behaviour compared to tension, with a gradual increase in stress up to the peak, followed by a descending branch indicating progressive material degradation. Figure 9c illustrates the shear stress-strain relationship, including an initial linear phase up to peak stress, followed by a sudden drop representing crack formation and sliding along mortar joints. The residual plateau suggests the presence of frictional resistance post-failure, often associated with aggregate interlock and roughness of joint interfaces.

3 Response analysis to acoustic and antrhopic vibrations

3.1 Description of the global FE model

The Circus Maximus, situated between the Aventine and Palatine hills, was an ancient Roman chariot-racing stadium and a hub for mass entertainment. As the largest venue for the famed "ludi romani", public games tied to Roman religious festivals. It measured 621 m in length and 118 m in width. The 3D FE model of the entire concert venue, spanning from the stage area to the Moletta tower, was developed using Midas FEA NX (Fig. 10). The soil layers and their properties were adopted according to the study done by Carpentieri et al. [43]. The soil layers were modelled using both 8-noded and 4-noded solid elements, ensuring contact between the tower masonry walls and the soil.

A linear elastic model was adopted for the soil, given the small displacement levels observed. Furthermore, historical records indicate that the soil has never exhibited signs of significant deformation, even during natural hazards such as earthquakes and flash floodings. Lateral boundary conditions were modeled using infinite elements, treating the boundaries as a continuous medium. This approach, following the work of Su and Wang [44], was adopted to effectively capture dynamic soil-structure interaction by minimizing wave reflection at the model boundaries, thereby enhancing the accuracy of the system's dynamic response simulation. The smallest crowd is represented by the green zone, indicating the area subjected to uniform pressure due to the applied loads. The number of individuals gradually increased until the red area became fully occupied. The main characteristics of the meshed model after convergence analysis are 52,229 nodes, 274,856 elements, 178,176 DOF, and 168,138 equations.

3.2 Soil properties of the circus maximus area

Young's and shear modules are derived from the Lamé coefficients which are obtained using the formulas described by Eqs. 3 and 4:

$$\lambda = \varphi(V_i^2 - V_s^2) \quad (3)$$

$$\mu = \varphi - V_s^2 \quad (4)$$

where, the key parameters governing wave propagation in the soil include the specific soil density (φ), the shear wave velocity (V_s), and the longitudinal wave velocity (V_l). Additionally, the mechanical behavior is characterized by Lamé coefficients: μ (shear modulus) and λ (first Lamé parameter). From Lamé coefficients λ and μ, it is possible to calculate

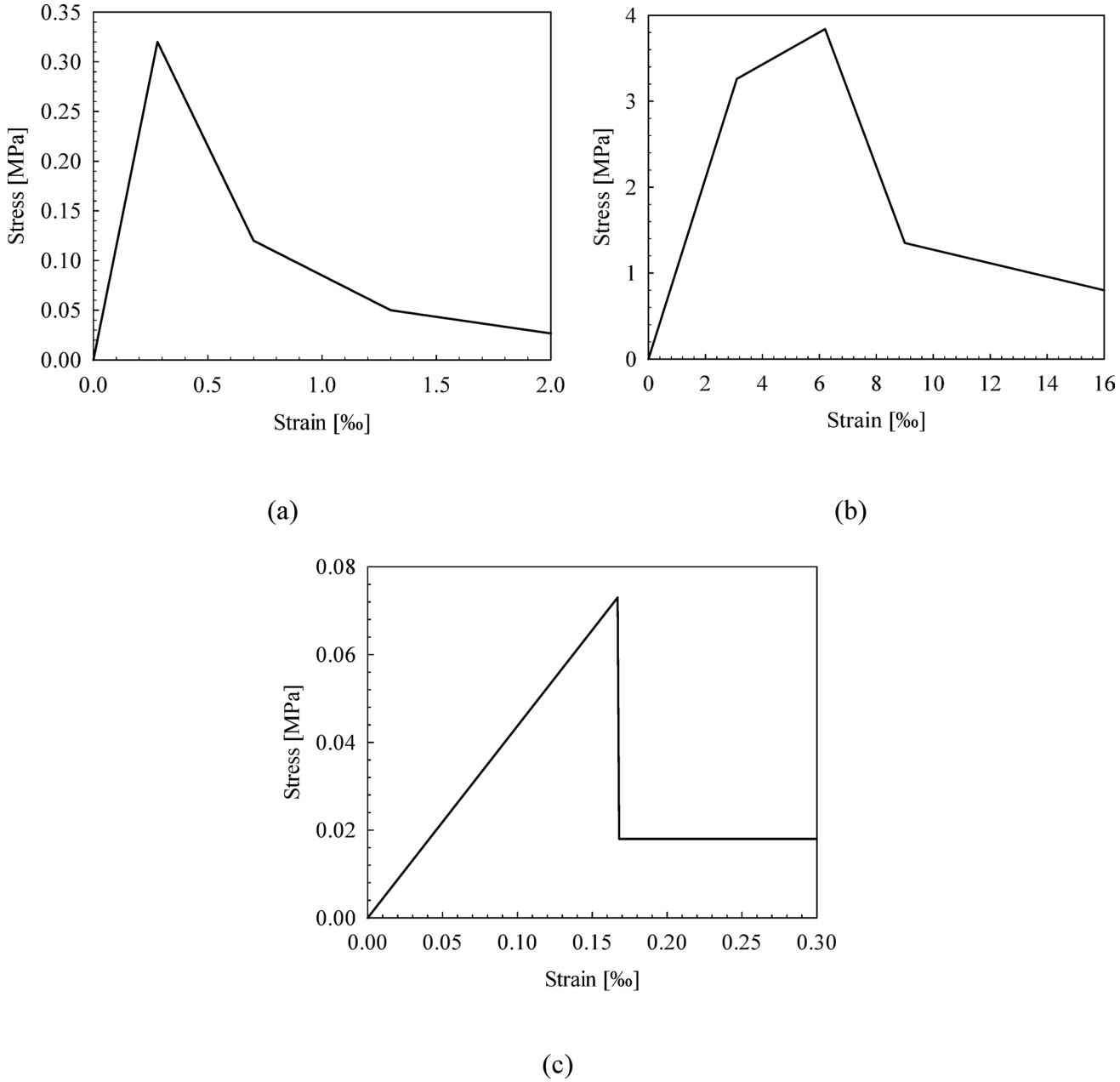


Fig. 9 Non-linear behaviour of masonry in **a** tension, **b** compression and **c** shear

the Young's modulus E and Poisson's ratio v using Eqs. 5 and 6, whereas the shear modulus is calculated by Eq. 7.

$$v = \frac{\lambda}{2(\lambda + \mu)} \tag{5}$$

$$E = \frac{\mu(\lambda + 2\mu)}{(\lambda + \mu)} \tag{6}$$

$$G = \frac{E}{2(1 + \nu)} \tag{7}$$

Table 6 represents the key properties of the soil model collected from different studies carried out in that specific area [31–33] and the calculated values of E, G, v.

In addition, another study investigated the fundamental frequencies of the soil, which were found to range from 1.2 Hz to 1.5 Hz [34]. Therefore, an iterative calibration procedure was carried out by varying the values of the mechanical properties reported in Table 9 until the average frequency of 1.35 Hz was reached. At the end of the calibration, the mechanical properties given in Table 7 were obtained, while the eigenfrequencies are 1.36 Hz for the 1st mode, 1.41 Hz for the 2nd, 1.49 Hz for the 3rd, and 1.54 Hz

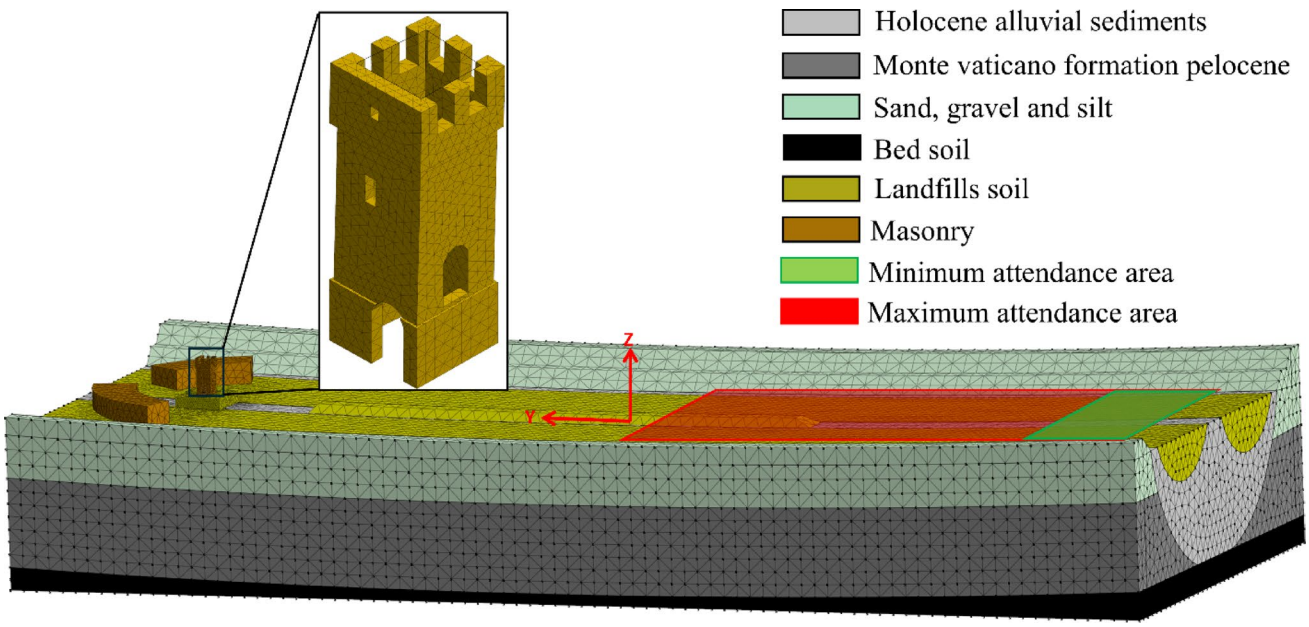


Fig. 10 3D FE model of the Circus Maximus including the soil and Moletta Tower

Table 6 Mechanical properties of stratified Circus Maximus soil

Soil type	ρ [kN/m^3]	C [Kpa]	Φ [°]	V_l [m/s]	V_s [m/s]	E [MPa]	G [MPa]	ν
Landfill consists of various mortar and concrete	18	0–10	27–30	1300±336	529±148	966,3–302,1	341,6–106,2	0.420
Holocene alluvial sediments	20	0	40	2002±398	582±158	991,3–385	372,1–131,3	0.458
Volcanic sediment (bed soil)	20.5	76	24	1791±337	473±81	671,8–338	229,1–115,4	0.467
Sand gravel and silt	20	0	40	1078	390	344.02	119.9	0.435
Monti Vaticano	20.5	76	24	1791±337	473±81	671,8–338	229,1–115,4	0.467

Table 7 Mechanical properties of Circus Maximus soil after calibration

Soil type	E [MPa]	G [MPa]	ν
Landfill consists of various mortars and concrete	407.0	143.3	0.420
Holocene alluvial sediments	434.7	149.1	0.458
Volcanic sediment (bed soil)	451.5	153.9	0.467
Sand gravel and silt	362.0	138.1	0.435
Monti Vaticano	405.0	167.4	0.467

for the 4th. It is worth noting that all frequencies fall within the range reported in [34].

3.3 Acoustic load modelling

Sound pressure is a change in pressure that results from the movement of sound waves as they travel through the air. These waves produce quasi-periodic pressure fluctuations that can be represented as a periodic load. The effective pressure of a sound wave is measured through the sound pressure level (SPL). The higher the SPL, the higher the sound intensity, and a potential damaging effect on nearby buildings.

To estimate the sound pressure propagating in open space, the sound intensity force during the concert event was measured at multiple distances. The relation between SPL, measured in dB, and the acoustic pressure, measured in Pa, is given by Eq. 8 [45, 46].

$$P_{Peak} = P_0 \cdot 10^{\frac{SPL1}{20}} \tag{8}$$

The reference pressure in a quiet environment (P_0=20 μPa), the peak pressure (P_{peak}), is corresponding to the sound pressure level at same position (SPL_1). The attenuation of sound pressure levels between two different positions is expressed by Eq. 9.

$$SPL_2 - SPL_1 = 20 \cdot \mathrm{Log}\left(\frac{r_1}{r_2}\right) \tag{9}$$

where r_1 and r_2 are the distances in meters from the source. The measured peak pressure levels showed significant attenuation due to the distance between the stage and the tower. The recorded SPL at the stage was 115 dB (11.25 Pa) and 85 dB (0.4 Pa) at the tower. This represents a 30 dB reduction in sound pressure level, corresponding to a 96% decrease in acoustic pressure. Since the frequency of the

periodic loading representing acoustic pressure constantly varies depending on the music, the worst-case scenario was simulated, considering a frequency of 3 Hz, which is close to the resonance frequency of the tower. Thus, the acoustic load is modelled as a pressure of 0.4 Pa uniformly distributed over the wall facing the stage (North-West) and applied for 30 s considering an impact time of 0.1 s and a frequency of 3 Hz. The FE simulation results show the dynamic effects along the tower's height. At the base, the peak acceleration was 1 mm/s2, increasing up to 2.5 mm/s2 at the top. On the other hand, peak particle velocity (PPV) is about 0.031 mm/s at the base and 0.115 mm/s at the top, corresponding to an amplification factor of 3.7. As expected, these results confirm that the dynamic response intensifies toward the structure's upper levels. Overall, given the modest values of accelerations and velocities, it is possible to conclude that the effect of acoustic pressure is negligible.

3.4 Anthropic load modelling

This subsection describes how the anthropic load generated from jumping during concerts is modeled and its effects on the tower. Besides crowd movement such as walking, the jumping motion represents the most critical scenario. Typical human motion frequencies vary from 2.0 to 3.2 Hz, which are close to the fundamental frequency of several structures. For instance, skipping of 1 to 2 min corresponds frequencies from 1.0 to 2.8 Hz, with peaks of 3.5 Hz for shorter times (20 s) [3].

In this study the motion of jumping on the spot with both feet simultaneously is considered since it is the worst load condition. For an idealized mathematical description and calculation of the forced vibrations, a half sinusoidal model was adopted. The half sinusoidal model is a sequence of semi-sinusoidal pulses modeled as shown in Eq. 10:

$$\begin{cases} F_s = K_p \cdot W \cdot \sin\left(\frac{\pi}{t_p} t\right) & 0 \le t \le t_p \\ F_s = 0 & t_p \le t \le T_p \end{cases} \tag{10}$$

where K_p represents the dynamic impact factor, $F_s(t)$ denotes the peak dynamic load, and W is the weight of a single person. The temporal characteristics are described by t_p, contact duration, and T_p, pace period, calculated as the inverse of the stepping frequency f_s. The impact factor K_p results from the condition of constant potential energy, meaning that the integral of the load-time function over one period must equalize the load at rest, which is the static weight (W) [3, 47] as shown in Eq. 11.

$$\int_0^{T_p} F_s(t)dt = W \cdot T_p \tag{11}$$

The resulting impact frequency increases with decreasing contact ratio t_p/T_p. According to experimental in this field, the contact ratio may vary between 0.25 and 0.6 and K_p ranges from 7 to 2.5. K_p can be determined as a function of the contact ratio as defined by [3]. When considering a large number of people jumping, the motion is not completely synchronized, which leads to a slightly longer contact duration of $t_p = 0.2$ s [48–50]. The relation between the contact ratio and jumping frequency can be expressed by Eq. 12.

$$\frac{t_p}{T_p} = 0.2 f_s \tag{12}$$

In this study, a weight of 800 N per person is considered, with a jumping frequency f_s of 2.7 Hz. The load duration is 3 min, emulating jumping for most of a song's length. The obtained dynamic impact factor K_p equals 2.8. Figure 11 shows the load function following the presented model.

To properly model the load generated by a group of people, it is necessary to determine the density of the attendees. Various codes and standards, such as ISO 10137 [51] and NBC2005, provide this information. Table 8 shows that the density of people in crowded areas during different events can vary between 3 and 6 people/m².

In the simulation, a load generated by 10,000 people jumping for 3 min was considered. The load was applied in the audience area close to stage and propagates through the soil according to the adopted soil model. Considering a density of 3 people/m², the attendance area is about 3,300 m^2. The nonlinear time history analysis revealed a maximum acceleration of 0.0547 m/s^2 at the top of the tower. Figure 12 shows the first 10 s of acceleration time history in the same position where sensor S_51 was located.

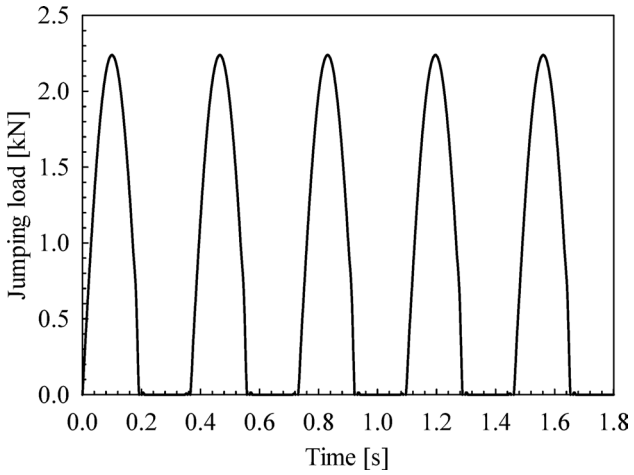


Fig. 11 Half sinusoidal model used to simulate the jumping load

Table 8 Density of people in crowded areas during the events

Activity	Crowd density [people/m²]	
	Common values	Maximum observed
Swaying (horizontal load), areas with seats	1	3
Swaying (horizontal load), areas without seats	1	6
Vertical actions for seated audience	1	6
Coordinated jumping (including jump dancing and rhythmic exercises), areas without seats	0.8	6
Coordinated jumping (including jump dancing and rhythmic exercises), areas without seats	1	6

3.5 Comparison between recorded accelerations and FE model

The results obtained with the FE model were compared to the accelerations recorded by the accelerometers. Obviously, the experimental signals also contained environmental noise and since the FE model results were obtained using only the jumping load as input, the measured accelerations had to be denoised. In addition, since the simulated loading condition is periodic and happens over a short period of time, while the actual load has a stochastic nature and occurs over a long period of time, a simplified statistical method was implemented. In detail, two scenarios were analysed. The first corresponds to environmental noise, considering records going from 12:00 a.m. to 7:00 a.m. UTC on the day before the concert. The second one corresponds to the 1 May concert event, considering records going from 5:00 p.m. to 10:30 p.m. UTC, which captured the anthropic vibrations. To distinguish the significant amplitudes from the environmental and electrical noise in the signal, a threshold based on the standard deviation (σ) of the noise was defined. Assuming the noise follows a Gaussian distribution with zero mean, by picking an interval of ± 3σ, 99.73% of noise values would be captured. This means that a threshold of ± 3σ ensures that the probability of exceedance is only about 0.27%. Through this method it was effectively possible to isolate high-amplitude accelerations. Thus, the mean absolute value of these peak accelerations outside the ± 3σ bound was calculated. Figure 13 shows the recorded accelerations, the ± 3σ thresholds, and the mean of the peak accelerations for both environmental and concert vibrations. It is noteworthy that human-induced crowd vibrations exhibited an amplitude increase of approximately four to five times compared to baseline environmental vibrations. Furthermore, the amplitude at the top of the tower was observed to be approximately twice the one at the base under environmental conditions, and nearly three times greater during concert-induced excitations.

Table 9 presents the maximum accelerations obtained after processing the data of all the sensors under environmental and concert vibrations.

The total acceleration includes all sources of vibration, while the ambient acceleration accounts for background vibrations unrelated to the concert. To isolate the input from the concert, the mean values of ambient acceleration were subtracted from the total accelerations. Table 10 presents acceleration measurements from multiple accelerometers (S_50, S_51, S_52, S_490, S_491 and S_53) during a concert event, comparing the total recorded acceleration, ambient acceleration, concert-induced acceleration, and accelerations obtained in numerical simulation. The last row of the table shows the relative error between the FE model predictions and the experimental data. Remarkably, the error was below 4% for all sensors, except at S_50, where it reached 16.70%. Overall, this discrepancy remains acceptable given that the difference is only 2.7 mm/s^2.

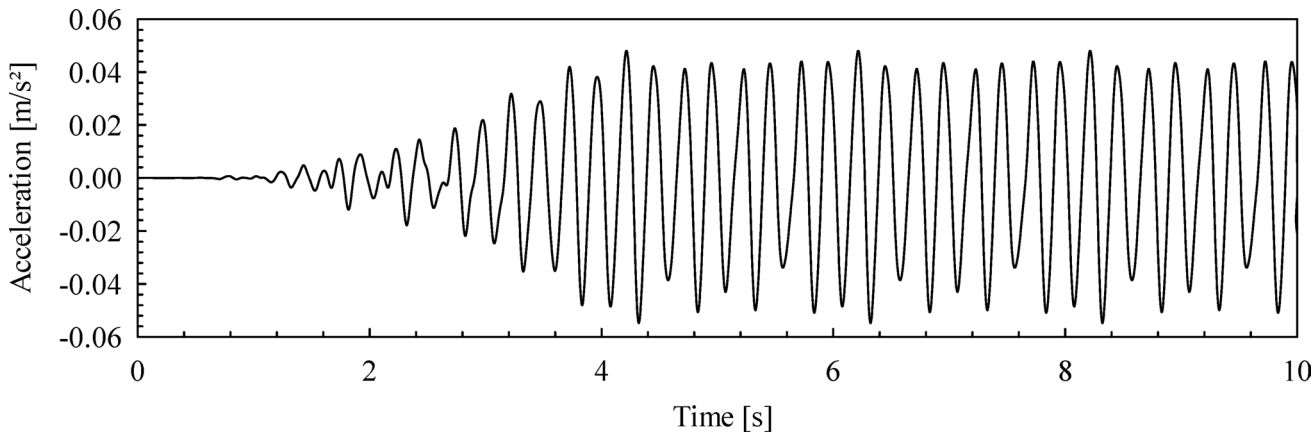
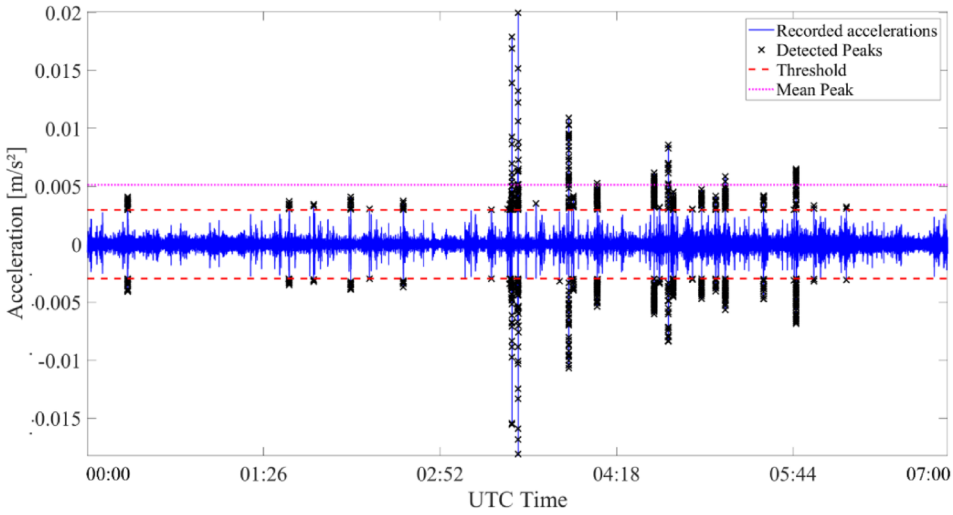
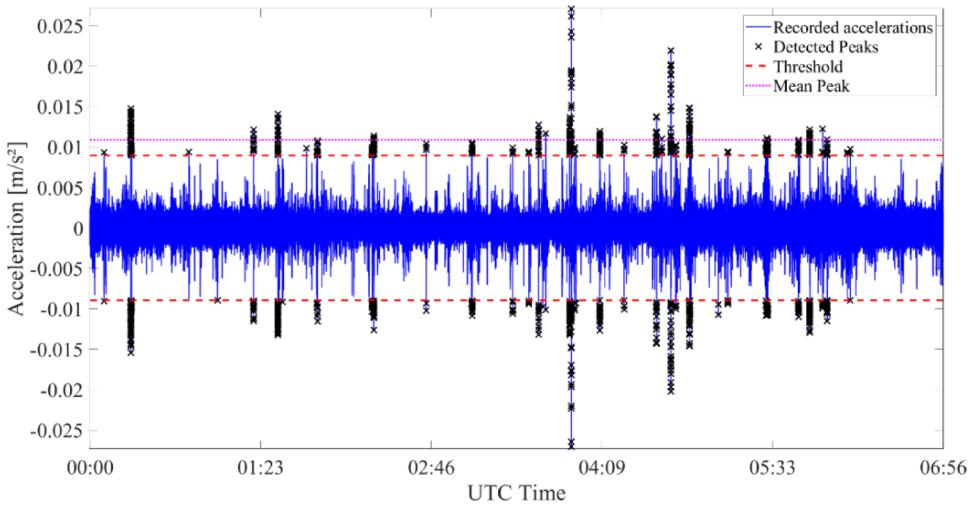


Fig. 12 Acceleration time history at the top of the tower obtained from the FE model considering 10,000 people jumping



(a)



(b)

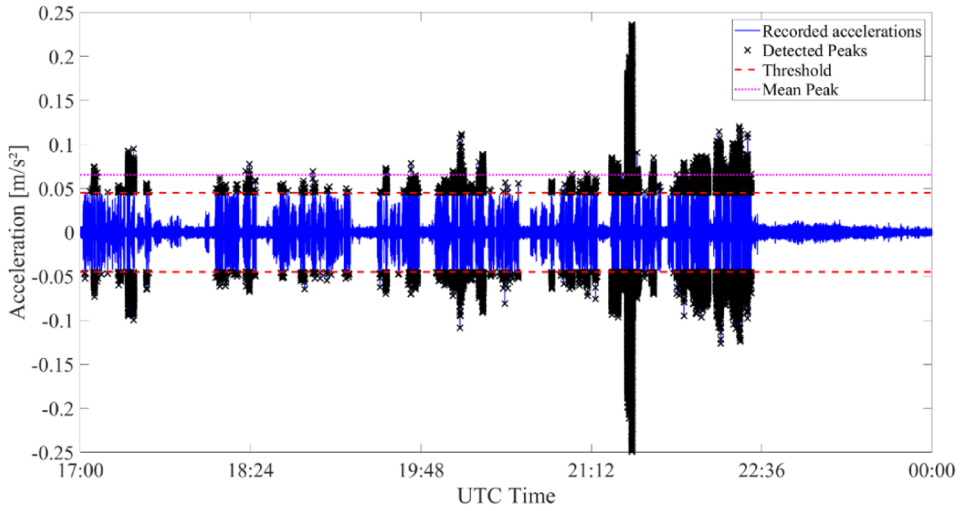
Fig. 13 Recorded accelerations: **a** environmental vibrations at the base, **b** environmental vibrations at the top, **c** concert vibrations at the base, and **d** concert vibrations at the top

3.6 Effect of large crowds on the structural safety of the tower

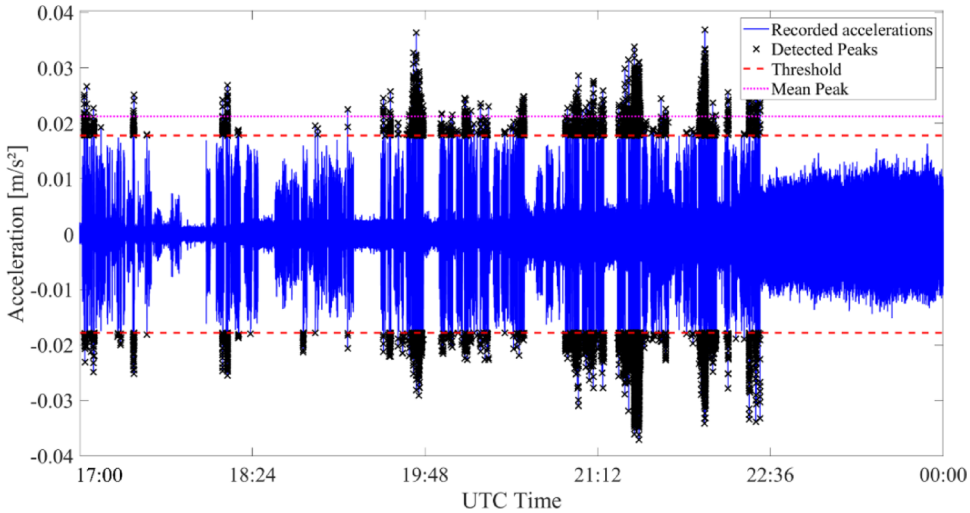
To assess the structural safety of the tower under different concert attendancscenarios, from 7,500 to 80,000 people, two analyses were carried out. The first was based on controlling the tower response in terms of peak particle velocity (PPV), whereas the second focused on tracking the formation of plastic hinges.

Various standards and codes [52, 53], have established PPV limits to avoid damage to historical structures. The main thresholds used as references are summarized in Table 11. The PPV recorded from FE analysis at different positions in the tower are compared to those suggested by the UNI 9916 code for the vibration of historical and ancient structures. Specifically, UNI-9916 indicates that for historical buildings, subjected to vibrations with frequencies less than 10 Hz, the velocity limits for short-term vibrations are 3.0 mm/s at the foundation and 8.0 mm/s at the top.

Figure 14 illustrates the impact of crowd size on the tower's dynamic response, showing how PPV increases with the number of people jumping. Notably, the PPV at the base follows an almost linear increment, while at the top of the tower it rises faster up to 50,000 people and then grows at a lower rate. Assuming a maximum capacity of 80,000 attendees, PPV reaches 14 mm/s at the top, compared to just 8 mm/s at the base. The FE analysis revealed that thresholds are exceeded when 36,000 people jump simultaneously. With this crowd size, the velocities reach 3.19 mm/s at the base and 8.9 mm/s at the top.



(c)



(d)

Fig. 13 (continued)

Table 9 Recorded accelerations under environmental and concert vibrations

		S_50	S_51	S_52	S_490	S_491	S_53
Environmental vibrations	Mean	0.0052	0.0110	0. 0071	0.0068	0.0091	0.0039
	Standard deviation	0.0015	0.0013	0.0010	0.0008	0.0010	0.0009
Concert vibrations	Mean	0.0213	0.0677	0.0518	0.0482	0.0622	0.1372
	Standard deviation	0.0017	0.0085	0.0107	0.0043	0.0080	0.0112

Table 10 Comparison of maximum accelerations obtained from SHM and FE model

	S_50	S_51	S_52	S_490	S_491	S_53
Total acceleration [m/s2]	0.0213	0.0677	0.0518	0.0482	0.0622	0.1372
Environmental vibrations [m/s2]	0.0052	0.0110	0. 0071	0.0068	0.0091	0.0039
Concert vibrations [m/s2]	0.0161	0.0567	0.0447	0.0414	0.0531	0.1333
FE model accelerations [m/s2]	0.0188	0.0547	0.0436	0.0403	0.0540	0.1290
Relative error [%]	16.70	3.53	2.46	2.66	1.69	3.23

Table 11 PPV limitations according to different standards

Standards and codes	Structure type	Limits values [mm/s]
UNI 9916	Historical buildings	3–8
DIN4150-3:1999 (Germany 1999)	Ancient architecture	3–10
BS7385-2 (UK 1993)	Ancient architecture	7.5
6.10SN640312:1992 (Switzerland 1992)	Old and poorly maintained buildings	2

The nonlinear history analysis revealed that plastic hinges first occur at the base level, precisely near the opening, due to the high-stress concentration under loading conditions equivalent to a crowd of 50,000 people (Fig. 15a). These early hinge formations indicate the inception of yielding. As the load was increased to simulate a scenario with 80,000 attendees, the plastic hinges propagated significantly, extending towards the opening on the South-East wall and further along the edges of the North-East wall (Fig. 15b). The plastic hinges formed at the base of the intermediate, thinner wall. Despite localised yielding is not indicative of structural failure, the analysis suggests a structural vulnerability under large crowd-induced loads, pointing out critical stress zones and potential failure mechanisms.

4 Conclusions

This study investigated the structural dynamics of the Moletta Tower, a historical masonry structure located in the Circus Maximus archaeological site in Rome, Italy. Using a calibrated three-dimensional FE model of the tower and the surrounding soil of the entire Circus area, the research evaluated how acoustic and anthropic vibrations generated

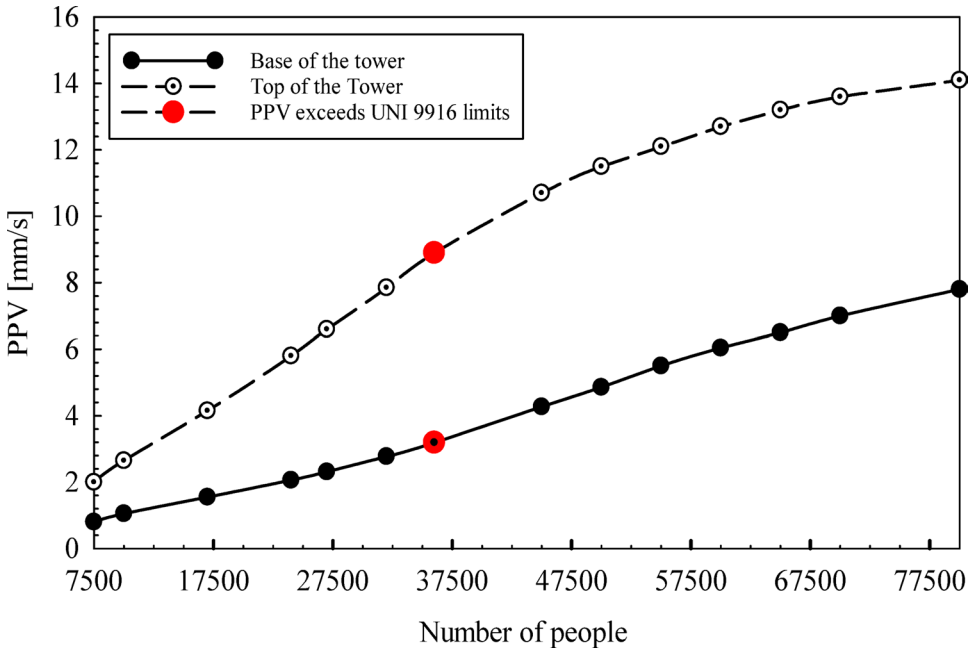


Fig. 14 FE simulated PPV at the base and at the top of the tower

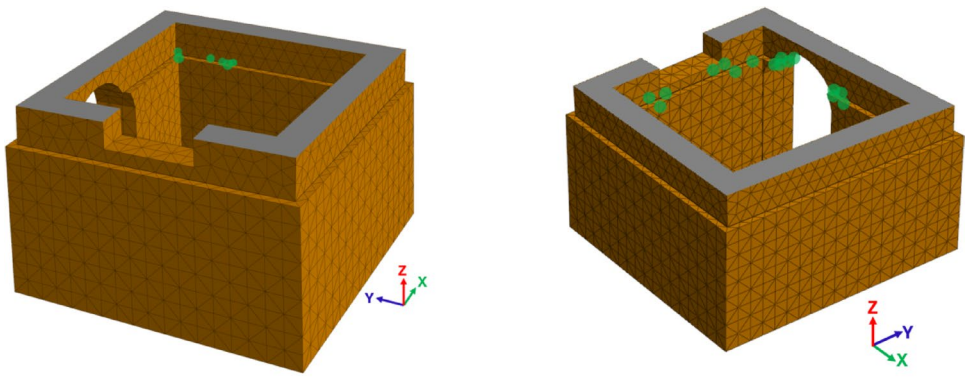


Fig. 15 Progressive plastic hinge formation for **a** 50,000 attendees and **b** 80,000 attendees

(a) (b)

during large concerts held at the venue might affect the historical structure.

The results showed that acoustic pressures, even at high intensities and close to resonance frequencies, produced minimal structural response due to the distance from the stage area, and can be considered negligible. In contrast, crowd-induced vibrations associated with jumping motion can pose potential structural issues. A sensitivity analysis on the crowd size revealed that the PPV at the top of the tower exceeded the thresholds recommended by UNI 9916 when more than 36,000 individuals were jumping simultaneously. Moreover, plastic hinges began to form at the base of the tower at crowd sizes exceeding 50,000, indicating localised yielding and stress concentrations, particularly near geometrical discontinuities such as openings and changes of wall section.

Inevitably, some assumptions and interpretations had to be made in the generation of the models. First, the assumption of uniform crowd density and simultaneous jumping may not fully reflect the actual concert conditions. Larger crowds might generate considerably lower loads if people are not jumping at the same time. This also depends on external factors such as the type of music or the average age of the audience. Therefore, the analysis is not intended to be unequivocally used to establish a limit on the maximum number of attendees. Secondly, a macro-modeling approach was adopted, in which masonry is treated as a homogeneous and isotropic material. This was necessary to reduce the computational demand of the nonlinear analysis, although it may overlook certain localized material variabilities. Nonetheless, these findings have important implications for the management of heritage sites used for public events. Specifically, they highlight the need for implementing real-time structural monitoring, advanced structural dynamics analyses and targeted intervention strategies to minimize the risk of damage. In conclusion, this study provides a robust framework for protecting cultural heritage in increasingly dynamic urban environments by combining numerical modeling with experimental validation.

Acknowledgements The authors would like to thank: Mauro Spampani and Alessandro Mitillo from Lunitek S.r.l (Italy) for providing the SHM sensors and their support in the data collection of the Moletta tower monitoring campaigns; the Capitoline Superintendence of Rome for their support during the Moletta tower monitoring campaigns.

Author contributions A. Bali: Methodology, Software, Validation, Writing—original draft, Writing—review & editing, Visualization. A. Cardoni: Conceptualization, Methodology, Writing—original draft, Writing—review & editing. A. R. Elahi: Formal analysis, Data curation, Writing—review & editing. M. A. Louar: Supervision. G. P. Cimellaro: Conceptualization, Project administration, Supervision, Writing—review & editing.

Funding Open access funding provided by Politecnico di Torino within the CRUI-CARE Agreement.

Data availability Data that supports the findings of this study is available upon reasonable request.

Declarations

Conflict of interest The authors declare that there is no conflict of interest regarding the publication of this article.

Open Access This article is licensed under a Creative Commons Attribution 4.0 International License, which permits use, sharing, adaptation, distribution and reproduction in any medium or format, as long as you give appropriate credit to the original author(s) and the source, provide a link to the Creative Commons licence, and indicate if changes were made. The images or other third party material in this article are included in the article's Creative Commons licence, unless indicated otherwise in a credit line to the material. If material is not included in the article's Creative Commons licence and your intended use is not permitted by statutory regulation or exceeds the permitted use, you will need to obtain permission directly from the copyright holder. To view a copy of this licence, visit http://creativecommons.org/licenses/by/4.0/.

References

1. Campisi T, Canale A, Tesoriere G, Lovric I, Čutura B (2019) The importance of assessing the level of service in confined infrastructures: some considerations of the old ottoman Pedestrian Bridge of Mostar. Appl Sci 9(8):8. https://doi.org/10.3390/app9081630
2. De Santis S, De Felice G (2014) Overview of railway masonry bridges with a safety factor estimate. Int J Archit Herit 8(3):452–474. https://doi.org/10.1080/15583058.2013.826298
3. Bachmann H, Ammann W (1987) Vibrations in structures: induced by man and machines, vol vol. 3. Iabse
4. Ji T, Ellis BR (1994) Floor vibration induced by dance-type loads: theory. Struct Eng 72:37
5. Bachmann H (1995) Vibration problems in structures: practical guidelines. Springer Science & Business Media
6. Racic V, Pavic A (2009) Mathematical model to generate asymmetric pulses due to human jumping. J Eng Mech 135(10):1206–1211. https://doi.org/10.1061/(ASCE)EM.1943-7889.0000044
7. S. Bulushev and A. Bunov, 'Dynamic analysis of strength and human-comfort level of the football stadium structures at coordinated movements of audience', in *MATEC Web of Conferences*, V. Andreev, T. Matseevich, A. Ter-Martirosyan, and A. Adamtsevich, Eds., 2018, p. 02032. https://doi.org/10.1051/matecconf/201819602032.
8. H. Sazak, 'Structural Health Monitoring Of A Stadium For Evaluating Human Comfort And Structural Performance'.
9. Peña F, Lourenço PB, Mendes N, Oliveira DV (2010) Numerical models for the seismic assessment of an old masonry tower. Eng Struct 32(5):1466–1478. https://doi.org/10.1016/j.engstruct.2010.01.027
10. Valente M, Milani G (2018) Effects of geometrical features on the seismic response of historical masonry towers. J Earthq Eng 22(sup1):2–34. https://doi.org/10.1080/13632469.2016.1277438
11. Altunişik AC, Okur FY, Genç AF, Guenaydin M, Karahasan O (2018) Automated model updating effect on the linear and nonlinear dynamic responses of historical masonry structures. Exp Tech 42:605–621
12. Valente M, Milani G (2016) Seismic assessment of historical masonry towers by means of simplified approaches and standard

FEM. Constr Build Mater 108:74–104. https://doi.org/10.1016/j.conbuildmat.2016.01.025
13. Ferrante A, Clementi F, Milani G (2019) Dynamic behavior of an inclined existing masonry tower in Italy. Front Built Environ 5:33
14. Zucchini A, Lourenço PB (2002) A micro-mechanical model for the homogenisation of masonry. Int J Solids Struct 39(12):3233–3255
15. Clementi F, Ferrante A, Giordano E, Dubois F, Lenci S (2020) Damage assessment of ancient masonry churches stroked by the Central Italy earthquakes of 2016 by the non-smooth contact dynamics method. Bull Earthq Eng 18:455–486
16. Milani G, Casolo S, Naliato A, Tralli A (2012) Seismic assessment of a medieval masonry tower in Northern Italy by limit, nonlinear static, and full dynamic analyses. Int J Archit Herit 6(5):489–524. https://doi.org/10.1080/15583058.2011.588987
17. Roca P, Cervera M, Gariup G, Pela' L (2010) Structural analysis of masonry historical constructions. Classical and advanced approaches. Arch Comput Methods Eng 17:299–325
18. Cardoni A, Cimellaro GP (2020) The role of reinforced concrete roofs in the seismic performance of masonry buildings. J Build Eng 28:101056. https://doi.org/10.1016/j.jobe.2019.101056
19. Lubliner J, Oliver J, Oller S, Oñate E (1989) A plastic-damage model for concrete. Int J Solids Struct 25(3):299–326. https://doi.org/10.1016/0020-7683(89)90050-4
20. Lee J, Fenves GL (1998) Plastic-damage model for cyclic loading of concrete structures. J Eng Mech 124(8):892–900. https://doi.org/10.1061/(ASCE)0733-9399(1998)124:8(892)
21. Borri A, Corradi M, Castori G, De Maria A (2015) A method for the analysis and classification of historic masonry. Bull Earthq Eng 13:2647–2665
22. Casolo S, Milani G, Uva G, Alessandri C (2013) Comparative seismic vulnerability analysis on ten masonry towers in the coastal Po Valley in Italy. Eng Struct 49:465–490
23. Valente M, Milani G (2018) Seismic response and damage patterns of masonry churches: seven case studies in Ferrara, Italy. Eng Struct 177:809–835
24. Casolo S (2017) A numerical study on the cumulative out-of-plane damage to church masonry façades due to a sequence of strong ground motions. Earthq Engng Struct Dyn 46(15):2717–2737. https://doi.org/10.1002/eqe.2927
25. Milani G, Valente M (2015) Failure analysis of seven masonry churches severely damaged during the 2012 Emilia-Romagna (Italy) earthquake: non-linear dynamic analyses vs conventional static approaches. Eng Fail Anal 54:13–56
26. Grillanda N, Chiozzi A, Milani G, Tralli A (2019) Collapse behavior of masonry domes under seismic loads: an adaptive NURBS kinematic limit analysis approach. Eng Struct 200:109517
27. Amador SDR, Brincker R (2021) Robust multi-dataset identification with frequency domain decomposition. J Sound Vib 508:116207. https://doi.org/10.1016/j.jsv.2021.116207
28. Günday F (2025) Structural health monitoring of steel garage model with stochastic subspace identification-covariance variance analysis. Buildings 15(6):6. https://doi.org/10.3390/buildings15060944
29. Romero-Sánchez E, Morales-Esteban A, Bento R, Navarro-Casas J (2023) Numerical modelling for the seismic assessment of complex masonry heritage buildings: the case study of the Giralda tower. Bull Earthq Eng 21(9):4669–4701. https://doi.org/10.1007/s10518-023-01714-x
30. Okuyucu D, Eslek T, Özdoğan DB, Laçin T, Mercimek Ö, Kocaman İ (2025) Dynamic identification and collapse mechanisms of unreinforced masonry Heritage: a comprehensive study of Erzurum Atatürk House. Eng Fail Anal 180:109850. https://doi.org/10.1016/j.engfailanal.2025.109850
31. Brancaleoni R, Celletti F, Garbin F, Padula G, Serio L, Spizzichino D (2015) Consolidation and restoration of the Moletta's Tower (Circus Maximus: Roma): site investigation and monitoring. In: Lollino G, Giordan D, Marunteanu C, Christaras B, Yoshinori I, Margottini C (eds) Engineering geology for society and territory - volume 8. Springer International Publishing, Cham, pp 335–338. https://doi.org/10.1007/978-3-319-09408-3_58
32. Moscatelli M et al (2014) Integrated geological and geophysical investigations to characterize the anthropic layer of the Palatine hill and Roman Forum (Rome, Italy). Bull Earthq Eng 12(3):1319–1338
33. Pagliaroli A, Quadrio B, Lanzo G, Sanò T (2014) Numerical modelling of site effects in the Palatine hill, Roman Forum, and Coliseum Archaeological Area. Bull Earthq Eng 12:1383–1403
34. Puzzilli LM, Bongiovanni G, Clemente P, Di Fiore V, Verrubbi V (2021) Effects of anthropic and ambient vibrations on archaeological sites: the case of the circus maximus in Rome. Geosciences (Basel) 11(11):463
35. Ministero delle Infrastrutture e dei Trasporti, *Norme tecniche per le costruzioni (NTC 2018)*, 2018.
36. Zienkiewicz OC, Taylor RL (2005) The finite element method for solid and structural mechanics. Elsevier
37. K.-J. Bathe, 'Frontiers in finite element procedures & applications', *Computational Methods for Engineering Science*, 2014.
38. Oden JT, Demkowicz L (2017) Applied functional analysis. Chapman and Hall/CRC
39. *Eurocode 3: Design of steel structures - Part 1–1: General rules and rules for buildings*. https://doi.org/10.1680/dsb.41721.011.
40. Cardoni A, Elahi AR, Cimellaro GP (2025) A refined output-only modal identification technique for structural health monitoring of civil infrastructures. Eng Struct 323:119210. https://doi.org/10.1016/j.engstruct.2024.119210
41. Allemang RJ (2003) The modal assurance criterion–twenty years of use and abuse. Sound Vib 37(8):14–23
42. Koutras AA, Shing PB (2021) Finite-element modeling of the seismic response of reinforced masonry wall structures. Earthq Eng Struct Dyn 50(4):1125–1146. https://doi.org/10.1002/eqe.3388
43. Carpentieri E, De Rita D, Monica GD (2015) Geology of the Murcia Valley and flood plain modifications in the construction of the Circus Maximus, Rome, Italy. Geoarchaeology 30(6):483–494. https://doi.org/10.1002/gea.21533
44. Su J, Wang Y (2013) Equivalent dynamic infinite element for soil–structure interaction. Finite Elem Anal Des 63:1–7. https://doi.org/10.1016/j.finel.2012.08.006
45. Dagdeviren OE (2018) Experiments to investigate the acoustic properties of sound propagation. Phys Educ 53(4):045007. https://doi.org/10.1088/1361-6552/aaaddc
46. S. Marchand, 'Avancées en modélisation spectrale du son musical (Advances in Spectral Modeling of Musical Sound)'.
47. Jones CA, Reynolds P, Pavic A (2011) Vibration serviceability of stadia structures subjected to dynamic crowd loads: A literature review. J Sound Vib 330(8):1531–1566
48. Roupa I, da Silva MR, Marques F, Gonçalves SB, Flores P, da Silva MT (2022) On the modeling of biomechanical systems for human movement analysis: a narrative review. Arch Comput Methods Eng 29(7):4915–4958. https://doi.org/10.1007/s11831-022-09757-0
49. Varela WD, Pfeil MS, de P. A. da Costa N (2020) Experimental investigation on human walking loading parameters and biodynamic model. J Vib Eng Technol 8(6):883–892. https://doi.org/10.1007/s42417-020-00197-3
50. Zhang Q, Chen W, Liang J, Cheng L, Huang B, Xiong C (2023) Influences of dynamic load phase shifts on the energetics and biomechanics of humans. R Soc Open Sci 10(8):230636. https://doi.org/10.1098/rsos.230636
51. I. O. for Standardization (2007) Bases for design of structures–serviceability of buildings and walkways against vibrations. ISO

52. DIN 4150–3 - Vibrations in buildings - Part 3: Effects on structures | GlobalSpec.
53. SN 640312A : 1992 Vibrations - vibration effects in buildings.

Publisher's Note Springer Nature remains neutral with regard to jurisdictional claims in published maps and institutional affiliations.